Journal of Luminescence 132 (2012) 2036–2042

Contents lists available at SciVerse ScienceDirect

Journal of Luminescence

journal homepage: www.elsevier.com/locate/jlumin

Synthesis, characterisation, luminescence and defect centres in solution combustion synthesised $CaZrO_3:Tb^{3+}$ phosphor

Vijay Singh [a,*], S. Watanabe [b], T.K. Gundu Rao [b], Katharina Al-Shamery [c], Markus Haase [d], Young-Dahl Jho [a,*]

[a] School of Information and Communications, Gwangju Institute of Science and Technology, Gwangju 500-712, Republic of Korea
[b] Institute of Physics, University of Sao Paulo, 05508-090 Sao Paulo/SP, Brazil
[c] Physical Chemistry, Institute for Pure and Applied Chemistry and Center of Interface Science University of Oldenburg, 26129 Oldenburg, Germany
[d] Department of Inorganic Chemistry I–Materials Research, Institute of Chemistry, University of Osnabrueck, Barbarastrabe 7, 49069 Osnabrueck, Germany

ARTICLE INFO

Article history:
Received 11 April 2011
Received in revised form
2 March 2012
Accepted 8 March 2012
Available online 27 March 2012

Keywords:
Phosphors
Combustion
Tb^{3+}
Photoluminescence
Defect centres

ABSTRACT

Tb^{3+} doped $CaZrO_3$ has been prepared by an easy solution combustion synthesis method. The combustion derived powder was investigated by X-ray diffraction, Fourier-transform infrared spectrometry and scanning electron microscopy techniques. A room temperature photoluminescence study showed that the phosphors can be efficiently excited by 251 nm light with a weak emission in the blue and orange region and a strong emission in green light region. $CaZrO_3:Tb^{3+}$ exhibits three thermoluminescence (TL) glow peaks at 126 °C, 200 °C and 480 °C. Electron Spin Resonance (ESR) studies were carried out to study the defect centres induced in the phosphor by gamma irradiation and also to identify the centres responsible for the TL peaks. The room temperature ESR spectrum of irradiated phosphor appears to be a superposition of two distinct centres. One of the centres (centre I) with principal g-value 2.0233 is identified as an O^- ion. Centre II with an axial symmetric g-tensor with principal values $g_{\parallel}=1.9986$ and $g_{\perp}=2.0023$ is assigned to an F^+ centre (singly ionised oxygen vacancy). An additional defect centre is observed during thermal annealing experiments and this centre (assigned to F^+ centre) seems to originate from an F centre (oxygen vacancy with two electrons). The F centre and also the F^+ centre appear to correlate with the observed high temperature TL peak in $CaZrO_3:Tb^{3+}$ phosphor.

1. Introduction

Alkaline-earth zirconates have attracted considerable attention due to their structural diversity and technological applications. Some perovskite compounds such as $SrZrO_3$, $CaZrO_3$ and $SrTiO_3$ are of particular interest because they exhibit remarkable protonic conductivity when they are doped with acceptor ions [1–5]. Moreover, materials with the perovskite structure are known to show superconductivity and remarkable electrical properties, including ferroelectricity and piezo-electricity [6–9]. Perovskite oxides having the general formula ABO_3 are getting special attention because of their applications in electrochemical devices such as capacitors, dielectric resonators for microwave, solid oxide fuel cells, oxygen sensors, oxygen separation membranes, hydrogen separators, hydrogen pumps, steam electrolysers, humidifiers and dehumidifiers, hydrogenation and dehydrogenation of hydrocarbons [1–15]. Among the alkaline earth zirconates, calcium zirconate is an interesting material for both mechanical and electrical applications such as filters, coatings, resonators and capacitors. $CaZrO_3$ ceramics have a relatively high permittivity and a high insulation resistance [8,16–18]. Also they show high ionic conductivity for solid electrodes in fuel cells and act as a microwave dielectric material [19]. It has been reported that for low cost applications, calcium zirconate can be considered as a good alternative to yttrium stabilized zirconia as it is a more stable compound than ZrO_2–CaO and shows good corrosion resistance [20,21]. Calcium zirconate based materials have excellent gas sensitivity at high temperature and hence they have been studied for their potential use as a high temperature thermistor material [22]. Its high sensitivity response to methane (CH_4) makes $CaZrO_3$ a potential candidate material for hydrocarbon sensing [23]. It has one of the most distorted structures and its high-pressure behaviour is of special interest [24]. However, there is not much work related to rare earth doped calcium zirconate with perovskite structure. It is noted that there are only few reports on the synthesis of $CaZrO_3$ by low temperature methods and also $CaZrO_3$ has not received much attention as a luminescent host. For a better knowledge of the energy level structure of $CaZrO_3$:Pr and $CaTiO_3$:Pr, a

* Corresponding authors. Tel.: +82 62 715 2292.
E-mail addresses: vijayjiin2006@yahoo.com (V. Singh), jho@gist.ac.kr (Y.-D. Jho).

0022-2313/$ - see front matter © 2012 Elsevier B.V. All rights reserved.
http://dx.doi.org/10.1016/j.jlumin.2012.03.027

spectroscopic study was carried out by Pinel et al. [25]. Yan et al. [26] reported a modified sol–gel method for the synthesis of rare earth composite ceramic phosphors $MM'O_3/CeO_2$ and $MM'O_3/CeO_2:Pr^{3+}$ (M=Ca, Sr; M′=Ti, Zr) with multicomponent hybrid precursors and found that the introduction of CeO_2 can enhance the luminescence intensity of $MM'O_3$ and $MM'O_3:Pr^{3+}$. Recently, Shimizu et al. [27] reported that Eu–Mg codoped and Tb–Mg codoped $CaZrO_3$ with perovskite structure, prepared using solid state sintering around 1400 °C, showed intense tricolour luminescence under UV excitation. In the present work, we have successfully employed a low temperature, simple, fast and safe combustion process for the synthesis of Tb^{3+} doped $CaZrO_3$ phosphor.

Radiation-induced defects in several phosphor materials and their role in their thermal, electrical and optical properties are well established. In a recent study of the photoluminescence (PL) properties of the perovskite-type stannates, it was suggested that the crystal structural distortion of host lattices is one of the key factors that determines PL intensity [27]. Accordingly, the increase of the crystal structural distortion, in other words, the enlargement of local contortion around rare earth ions, would enhance the PL intensity in the rare earth doped perovskite oxides.

$CaZrO_3$ forms a perovskite-type structure like $CaSnO_3$ but its structure is more distorted than that of $CaSnO_3$ [27]. Therefore, it is anticipated that $CaZrO_3$ has the potential for a favourable host lattice for synthesis of rare earth doped phosphors. Rare earth ions in general are known to yield good luminescence when used as dopants in different host matrices. Among the lanthanides ions, Tb, especially in its 3+ oxidation state, gives a good green luminescence yield, under UV excitation. In this study, we carried out Tb doping into $CaZrO_3$ and examined its basic photoluminescence and thermoluminescence (TL) properties.

TL and TL–ESR correlation studies of Tb^{3+} doped $CaZrO_3$ have not been reported yet. It has been known for a long time that the phosphor coating in devices is continuously hit by ionising radiations in order to convert to visible light output. In such a situation, the formation of defect centres can be expected. In this respect, a study of radiation induced defects and knowledge about the type of defects are of a great practical importance. In view of this, in the present investigation TL and ESR studies of Tb^{3+} doped $CaZrO_3$ phosphor are carried out to identify the defect centres. In addition, the prepared sample was characterised by X-ray diffraction (XRD), field emission scanning electron microscopy (FESEM) and photoluminescence (PL) techniques.

2. Experimental

2.1. Synthesis

The powder sample of $CaZrO_3:Tb_{(0.03)}$ phosphor was synthesised by the combustion technique. For the combustion, a fuel and oxidisers are required. In the present synthesis, metal nitrates are used as the oxidiser and urea is employed as the fuel. Stoichiometric compositions of metal nitrates and fuel are calculated based upon propellant chemistry. Thus, the heat of combustion is maximum for oxidiser/fuel ratio 1 [28]. The following precursors were employed: calcium nitrate ($Ca(NO_3)_2\cdot 4H_2O$, 99%, Aldrich), zirconium nitrate ($ZrO(NO_3)_2\cdot 2H_2O$, 99%, Kanto Chemical Co.), terbium nitrate ($Tb(NO_3)_3\cdot 5H_2O$, 99.9%, Aldrich) and urea ($CO(NH_2)_2$, 99%, Aldrich) all were weighed according to the stoichiometry. The precursors were dissolved in a minimum amount of distilled water and allowed to react at 60 °C for 20 min to obtain a homogenous solution. Then the solution was introduced into a muffle furnace preheated to 550 °C. Within a few minutes, the solution boiled, ignited and produced a self-propagating flame. The products obtained by the combustion process were fluffy masses and these were crushed into a fine powder. The product of the combustion reaction was then given an annealing treatment at 1000 °C for 4 h in an open crucible in air to remove by-products and reduce internal strain before it was used for further characterisation.

2.2. Characterisation

The phase composition of the synthesised powder was analysed by XRD using a Bruker D8 advance powder diffractometer (CuK_α radiation) in the 2θ range of 5°–80°. The morphology of the powders was determined using a JEOL-JSM-700F scanning electron microscope (FE-SEM). FT-IR spectra were taken using a Perkin-Elmer Rx1 instrument in the range from 4000 to 400 cm^{-1}. The room temperature photoluminescence (PL) of the prepared phosphors was studied using a JASCO, FP-6500, spectrofluorometer.

Irradiation of the samples was carried out using a ^{60}Co gamma source. A Daybreak 1100 series automated TL reader system was utilised for TL experiments which were carried out in a nitrogen atmosphere with a heating rate of 5 °C/s. Electron Spin Resonance experiments were carried out using a Bruker EMX ESR spectrometer operating at X-band frequency with 100 kHz modulation frequency. Diphenyl Picryl Hydrazyl (DPPH) was used for calibrating the *g*-factors of defect centres. Temperature dependence of the ESR spectra was studied using a Bruker B VT 2000 variable temperature accessory.

3. Results and discussions

3.1. X-ray diffraction

Fig. 1 shows the X-ray diffraction pattern of $CaZrO_3:Tb^{3+}$ phosphor. The XRD pattern shows well-defined peaks, which indicate a high crystallinity of the synthesised compound. All the reflections in Fig. 1 could be indexed to those of standard orthorhombic $CaZrO_3$ (JCPDS File No. 76-2401) phase in addition to weak reflex (■) lines which might belong to intermediate phases [29–31]. It has been reported that calcium zirconate formation starts at temperature ~900 °C and proceeds up to 1500 °C [32]. Also phase-pure $CaZrO_3$ is reported not to form in low temperature synthesis processes and weak reflections of ZrO_2 and $CaZr_4O_9$ phases were identified by earlier workers [29–32].

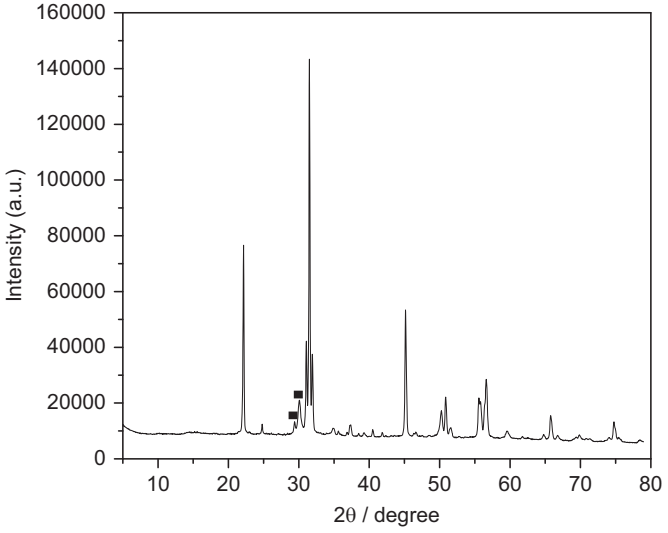

Fig. 1. Powder XRD pattern of $CaZrO_3:Tb^{3+}$ phosphor.

This result indicated that the crystalline and orthorhombic phase of $CaZrO_3$ could be obtained by using the urea-assisted combustion method.

3.2. FT-IR

The presence of water and organic residues in the $CaZrO_3:Tb^{3+}$ phosphor was investigated by IR spectral analysis. Fig. 2 shows the FT-IR spectrum of the $CaZrO_3:Tb^{3+}$ phosphor. Common bands do not exist in the spectrum such as the broad O–H band around 3400 cm^{-1}, the 1630 cm^{-1} H_2O vibrational band or the bands related to NO_3^- groups at 1384 cm^{-1}. This indicates that the nitrates used in the starting materials were completely eliminated and that the product is free of water. There is no evidence for the presence of any organic intermediates in the sample. Prasanth et al. [33] have reported a similar IR spectrum. They reported a broad absorption peak at 3440 cm^{-1} due to the presence of adsorbed moisture which is absent in our sample. Our present results are also supported by the IR spectrum given by Perry et al. [34]. Other authors have investigated in detail the IR spectra of $CaZrO_3$ powders calcined at different temperatures [29,30,35].

3.3. Scanning electron microscopy

The powder morphology of the combustion synthesised powders was characterised by the FE-SEM technique. Fig. 3a–c presents FE-SEM images of the powder under various magnifications. At low magnification, as shown in Fig. 3a and b, the FE-SEM image shows very clearly that the crystallites have no uniform shapes and sizes. Also, there are some crystals containing pores and cracks while some do not. This irregularity in size, shape and porosity is caused by the inhomogeneous heat and mass flow in the flame during the combustion process. The pores and cracks could be expected due to the evolution of large amounts of gas during the low temperature combustion process. The FE-SEM image also shows the existence of small particles which is the inherent nature of combustion synthesised products. The high resolution FE-SEM image (Fig. 3c) is similar to images of FE-SEM studies published previously [29,36–38].

3.4. Photoluminescence

Fig. 4(a) and (b) shows photographs of the $CaZrO_3:Tb^{3+}$ powders prepared by the combustion method under room light and UV (254 nm) radiation respectively. The $CaZrO_3:Tb^{3+}$ phosphor presents a light brown powder which emits green light under an UV-source. Fig. 5 shows the emission and excitation spectra of the $CaZrO_3:Tb^{3+}$ phosphor. Fig. 5(a) shows the excitation spectrum of a sample by monitoring the strongest 545 nm ($^5D_4 \rightarrow {}^7F_5$) emission of the Tb^{3+} ion. The excitation spectrum is a combination of a broad band and several narrow peaks. There are two bands: the main

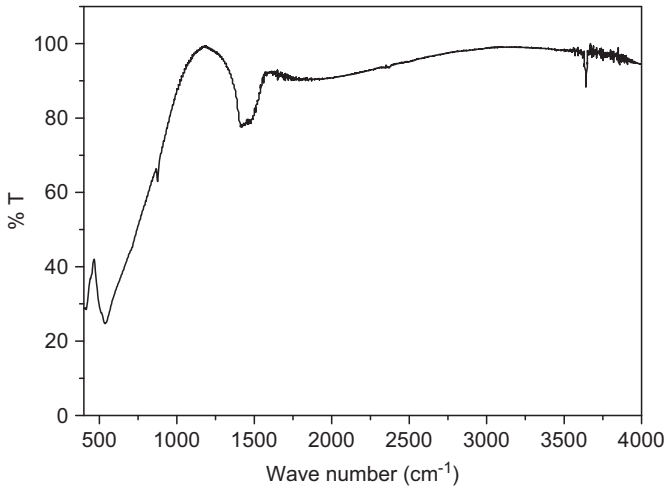

Fig. 2. FT-IR spectrum of the $CaZrO_3:Tb^{3+}$ phosphor.

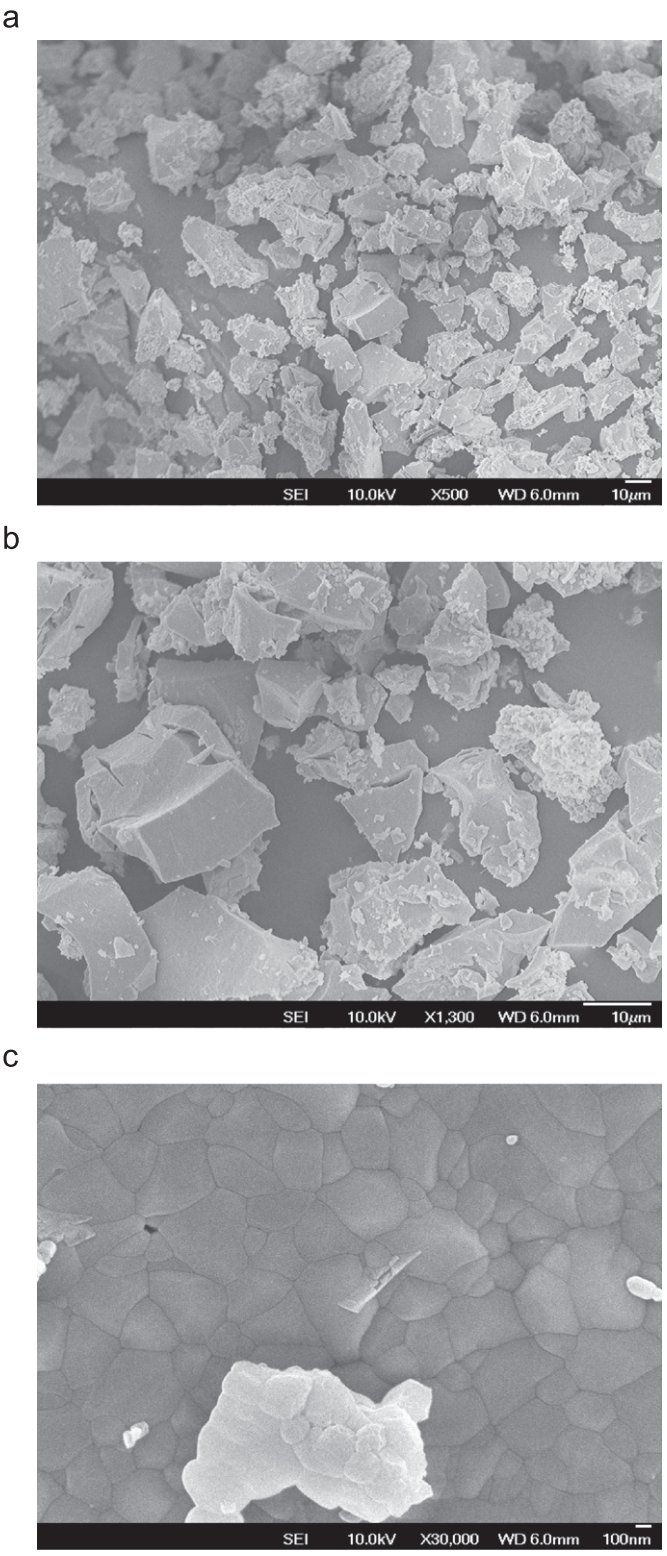

Fig. 3. SEM images of the $CaZrO_3:Tb^{3+}$ phosphor at low and high magnification. (a), (b), and (c) correspond to magnification × 500, × 1300 and × 30000 respectively.

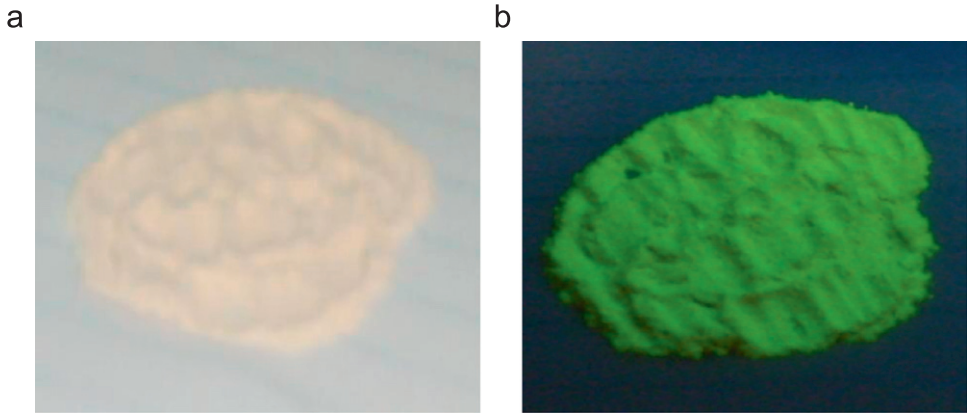

Fig. 4. Typical photographs of a $CaZrO_3:Tb^{3+}$ phosphor sample under (a) room light (appearance: a light brown powder) and (b) UV-254 nm (appearance: green emission of Tb^{3+}).

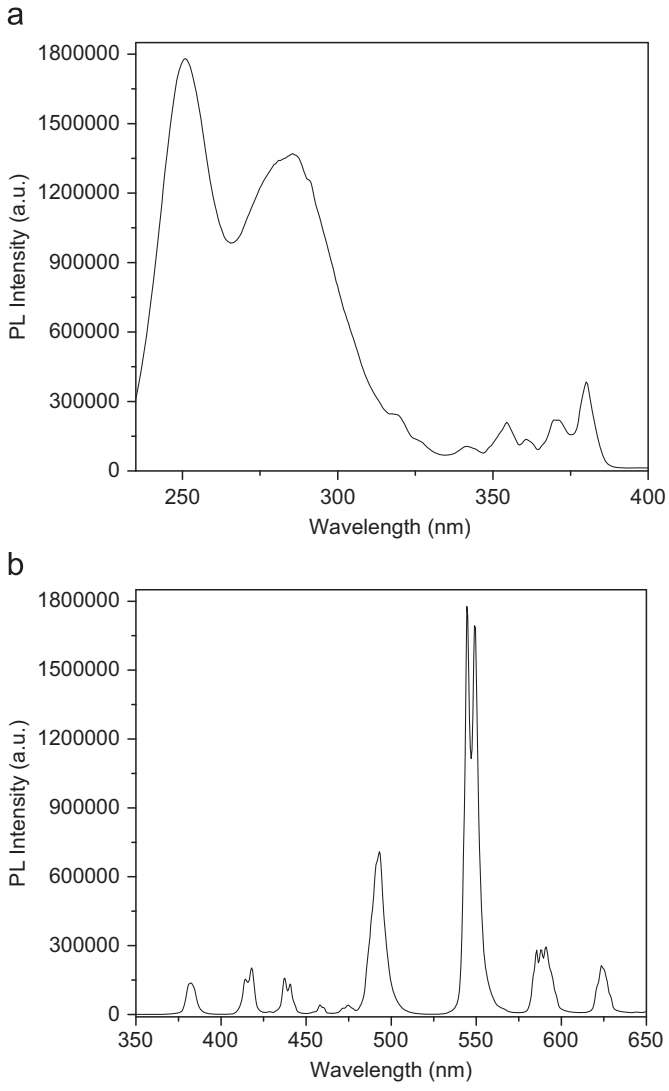

Fig. 5. Photoluminescence spectra of the $CaZrO_3:Tb^{3+}$ phosphor: (a) excitation spectrum for emission at 545 nm and (b) emission spectrum for excitation at 251 nm.

excitation peak appeared at around 251 nm and another peak with maximum at 285 nm was observed in the range from 240 to 325 nm. The former one was more intense than the latter one. These peaks overlap with each other and are not resolved well. Zhang et al. [39] observed band peaking at 250 nm in the undoped and Tm doped $CaZrO_3$ phosphor and they reported that this is due to the existence of defect level in the host. In the same report they mentioned that similar excitation and absorption peaks due to the defect levels also exist in Eu doped $SrZrO_3$ [40] and Tm doped $SrHfO_3$ [41] phosphors. We presume that another band peaking at 285 nm represents the spin allowed 4f–5d transition (f–d transition) of Tb^{3+} ions. The other sharp peaks in the range from 325 to 400 nm are due to 4f–4f transition of Tb^{3+} ions. The emission spectrum recorded under 251 nm excitation is shown in Fig. 5(b). The emission spectrum exhibits four major emission bands at around 493, 545, 591 and 623 nm, which are attributed to the typical $^5D_4 \rightarrow {}^7F_6$, $^5D_4 \rightarrow {}^7F_5$, $^5D_4 \rightarrow {}^7F_4$ and $^5D_4 \rightarrow {}^7F_3$ transitions of Tb^{3+} ions respectively. Also weak blue emission peaks with the wavelengths below 480 nm were observed originating from the $^5D_3 \rightarrow {}^7F_j$ (6, 5, 4, 3, 2, 1 and 0) transition of Tb^{3+} ions. Among these transitions, the green emission at 545 nm ($^5D_4 \rightarrow {}^7F_5$) is the most intense and the luminescence can be seen by the naked eye under UV radiation as mentioned above. Similar emission spectra have been reported by Shimizu et al. [27]. The photoluminescence investigation of the $CaZrO_3:Tb^{3+}$ powder phosphor confirms that this phosphor presents a potential green luminescent optical material for green luminescent display systems.

3.5. TL and ESR

Prior to gamma irradiation no glow peaks were observed in $CaZrO_3:Tb^{3+}$ sample. The TL glow curve of the $CaZrO_3:Tb^{3+}$ phosphor for a test gamma dose of 10 Gy is shown in Fig. 6. The main TL peak occurs at about 480 °C with smaller peaks at 126 °C and 200 °C. A heating rate of 5 °C/s has been used for recording the glow curves.

The ESR spectrum at room temperature of gamma irradiated (dose: 10 kGy) Tb^{3+} doped $CaZrO_3$ is shown in Fig. 7. Thermal annealing experiments indicate that at least two defect centres contribute to the observed ESR spectrum. These defects are labelled in Fig. 7. The ESR line labelled as I is due to a centre characterised by an isotropic *g*-value equal to 2.0233 and 30 G linewidth. Centre I has a relatively large linewidth which indicates unresolved hyperfine structure. This is due to the interaction of the unpaired electron with nearby nuclear spins. In $CaZrO_3$, calcium (^{43}Ca) as well as zirconium (^{91}Zr) have isotopes with nuclear spin. ^{43}Ca has a nuclear spin 7/2 (magnetic moment: 1.3173) with 0.14% abundance. On the other hand, ^{91}Zr (nuclear spin 5/2 and magnetic moment: 1.3036) has an abundance of 11.2% [42]. Therefore, the possibility of the electronic spin

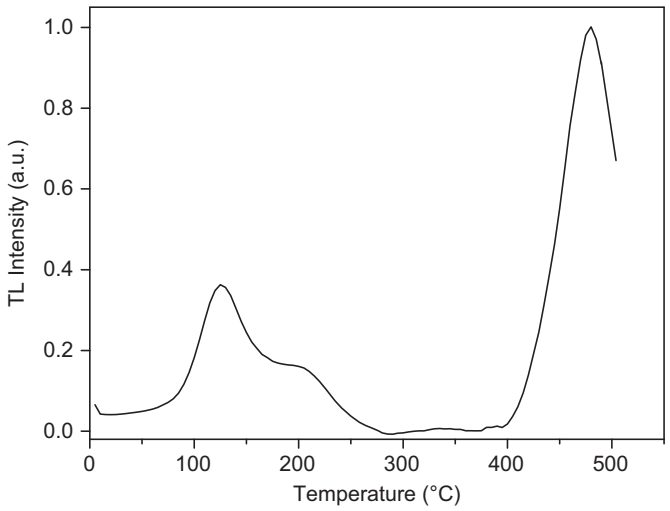

Fig. 6. TL glow curve of $CaZrO_3:Tb^{3+}$ phosphor (test gamma dose: 10 Gy).

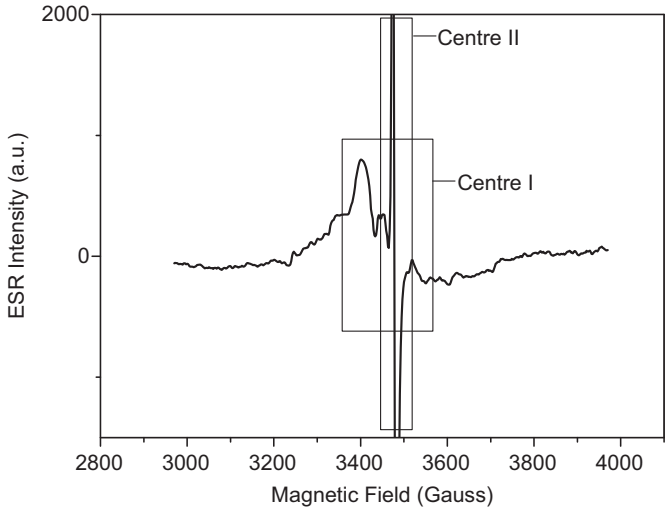

Fig. 7. Room temperature ESR spectra of irradiated $CaZrO_3:Tb^{3+}$ phosphor (gamma dose: 10 kGy). Line labelled as I is due to an O^- ion. Centre II line is assigned to a F^+ centre. Spectrometer conditions for recording the spectrum are—microwave power: 32 mW; modulation amplitude: 4 G and scan range of 1000 G.

interacting with zirconium ion (^{91}Zr) is more due to the ion's larger abundance.

$CaZrO_3$ is an orthorhombic perovskite ABO_3 compound belonging to the space group Pbnm [43]. $CaZrO_3$ consists of slightly deformed ZrO_6 octahedra with Zr–O bond lengths ranging from 2.09 to 2.10 Å and O–Zr–O angles in the range 88–90.9°. The average Zr–O–Zr tilt angle between ZrO_6 octahedra is 146°. In an ideal cubic perovskite structure, B–O–B angles between the corner sharing [BO_6] octahedra are 180° and the divalent A^{2+} cation resides in a dodecahedral site with m3m site symmetry, coordinated to 12 oxygen atoms. The rotation of [ZrO_6] octahedra distorts the Ca site with a reduction in site symmetry from Pm3m to1 and the coordination of Ca reduced from 12 to 8 with Ca–O bond lengths ranging from 2.341 to 3.625 Å. $CaZrO_3$ is one of the most distorted orthorhombic Ca-oxide perovskites. The divalent Ca^{2+} cation resides in a distorted dodecahedral site.

Mixed occupancy is expected at Zr site with partial replacement by Ca atoms. Hence, a number of trapping sites for the electron and hole on irradiation are created due to antisite formation which results from the interchange of the ions on octahedral and dodecahedral positions by divalent and tetravalent ions. Moreover, a change in the charge state of defect centres and impurities in the lattice is possible due to damage created by irradiation [44]. Many of the optical and luminescence properties of the crystal are affected by these defects.

Cation disorder as well as non-stoichiometry of $CaZrO_3$ can lead to a large number of lattice defects, which may serve as trapping centres. In this situation, irradiation can form F^+ centres by trapping electrons at oxygen vacancies. On the other hand, O^- ions can be formed by hole trapping at calcium or zirconium vacancies. The observed relatively large linewidth of centre I indicates that the unpaired electron is delocalised and interacts with nearby zirconium nuclei. Hence centre I is assigned to an O^- centre stabilized by a nearby cation vacancy (a hole trapped in a Ca^{2+}/Zr^{4+} ion vacancy).

The stability of centre I was measured using the pulsed-thermal annealing method. After heating the sample up to a given temperature, where it is maintained for 3 min, it is cooled rapidly down to room temperature and ESR experiments were carried out at room temperature. Fig. 8 shows the thermal annealing behaviour of centre I. It is seen that the centre becomes unstable around 80 °C and decays in the temperature range 80–200 °C. This decay appears to be related to the TL peak at 126 °C.

Fig. 9 shows the ESR spectrum of centre II. This spectrum has been recorded with the following spectrometer conditions—microwave power: 32 mW; modulation amplitude: 1 G and scan range of 100 G. Centre II is characterised by an axial symmetric g-tensor with principal values $g_{\parallel}=1.9986$ and $g_{\perp}=2.0023$. In an earlier study on an oxide system, yttria stabilized zirconia (YSZ), i.e. ZrO_2:Y, Costantini et al. [45] have observed a centre with principal values $g_{\parallel}=1.996$ and $g_{\perp}=1.972$. The g-values in YSZ are found to be smaller than the free-electron value and the centre has been attributed to an F^+ centre, i.e. a singly charged oxygen vacancy with one remaining electron. Costantini et al. suggested a symmetry breaking defect at an anionic site near the F^+ centre to explain the axial nature of the g-tensor. This anionic site defect assigned to a neutral F centre (oxygen vacancy with two electrons) appears to be consistent with the large density of oxygen vacancies present in the YSZ system. On the basis of the results of Costantini et al., the defect centre II in $CaZrO_3:Tb^{3+}$ phosphor is assigned to an F^+ centre which needs to be in the proximity of an F centre. The axial nature of the g-tensor could result from an F centre present near the vicinity of centre II in a manner similar to the YSZ. The basic lattice of $CaZrO_3$ may contain oxygen vacancies as mentioned earlier and this can lead to the formation

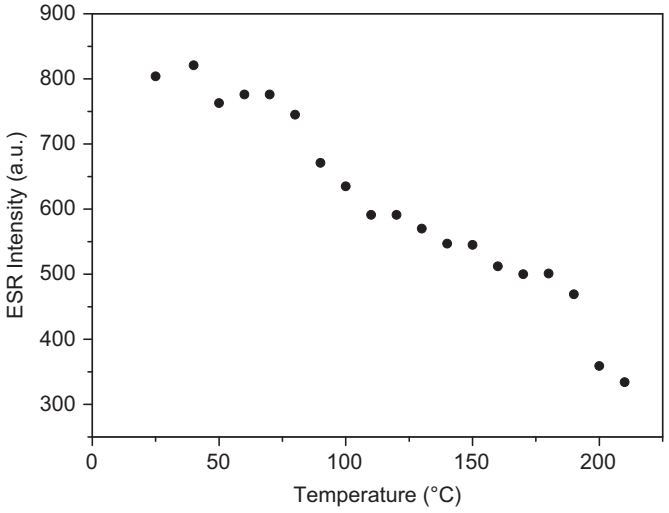

Fig. 8. Thermal annealing behaviour of centre I in $CaZrO_3:Tb^{3+}$ phosphor.

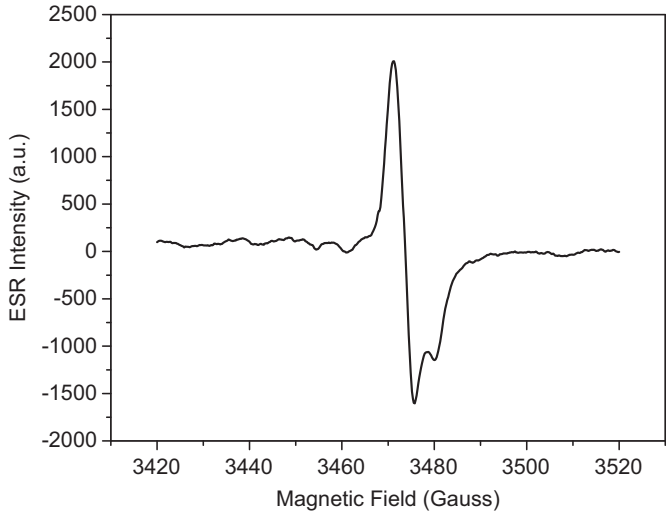

Fig. 9. ESR spectrum of centre II in irradiated $CaZrO_3:Tb^{3+}$ phosphor. The spectrum has been recorded with the following spectrometer conditions—microwave power: 32 mW; modulation amplitude: 1 G and scan range of 100 G.

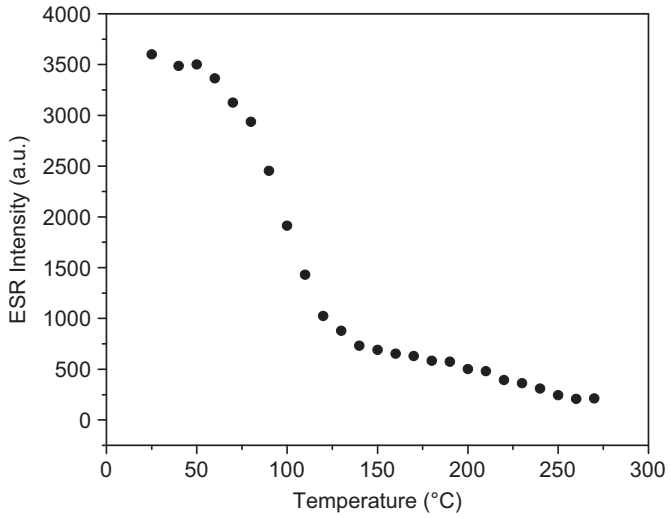

Fig. 10. Thermal annealing behaviour of centre II in $CaZrO_3:Tb^{3+}$ phosphor.

of F centres in close proximity to centre II. It may be mentioned that in a recent review Popov et al. [46] have discussed in detail the production mechanisms of F centres in oxide and halide systems.

Fig. 10 shows the thermal annealing behaviour of centre II. It is observed that the centre becomes unstable near 50 °C and starts to exhibit a two-step decay. The first stage of decay is pronounced and is in the temperature range 50–150 °C. The second step of decay occurs in the 150–260 °C temperature region. Centre II along with centre I appears to be associated with the low temperature TL peak at 126 °C. There seems to be a similarity between the decay of centre I and first stage decay of centre II even though the decay of centre II in the low temperature range is more pronounced. This indicates that centre II may be acting as a recombination centre when the hole from O^- ion (centre I) is released and recombines with the electron in F^+ centre. On the other hand, the second stage of decay of centre II indicates that it could also be related to the TL peak observed around 200 °C.

Thermal annealing experiments have shown that the two centres observed in the irradiated phosphor decay below 300 °C. A new centre (centre III) has been observed during high temperature thermal annealing experiments. The ESR spectrum after thermal annealing at 400 °C is shown in Fig. 11. The intensity of the new ESR line is found to be relatively small. Centre III has an isotropic g-factor equal to 2.0045 with a 6 G linewidth and is tentatively assigned to an F^+-centre based on the reasons mentioned earlier. A similar formation behaviour like centre III is exhibited by the E_1' centre (an oxygen vacancy having an unpaired electron localised in the sp^3 hybrid orbital extending into the vacancy from the adjacent silicon ion) in SiO_2 lattice. In a detailed investigation on the formation and thermal annealing characteristics of E_1' centre in SiO_2, Jani et al. [47] have proposed an oxygen vacancy containing two electrons as the precursor of the E_1' centre. It was suggested that this oxygen vacancy with two electrons is likely to release an electron during post-irradiation heating resulting in the formation of E_1' centre. On the basis of these results in SiO_2, it is speculated that in $CaZrO_3:Tb^{3+}$ phosphor the formation process of centre III might be similar.

Oxygen vacancies can be present in $CaZrO_3$ lattice due to non-stoichimetry and impurities. Room temperature irradiation can convert these vacancies into F-centres. F-centres contain two electrons and during heating release an electron which appears in the thermal annealing experiments as an appearance of centre III. Jani et al. [47] have observed only one type of E_1' centre, while two distinct F^+ centres are seen in the present study. Three basic differences are observed for the F^+ centres observed in this study. The g-values are different. Centre II is perturbed by a nearby F centre which leads to an axially symmetric g-tensor. On the other hand, centre III is characterised by an isotropic g-value. The formation processes of the two centres are different. Centre II is formed by the capture of an electron at an anionic vacancy while centre III results when sufficient thermal energy is given to an F centre (an anion vacancy with two trapped electrons) causing it to release one of the electrons. The thus formed F^+ centre releases the unpaired electron only at higher temperatures and hence has higher thermal stability as compared to centre II.

The thermal annealing behaviour of centre III is shown in Fig. 12. It is seen that centre III grows in the temperature region 300–490 °C. The decay of centre III beyond 490 °C corresponds to the decay of the F^+ centre. The present results indicate that the precursor of centre III (F-centre) and also the F^+ centre appear to correlate with the high temperature TL peak at 480 °C in the phosphor. These centres release electrons during thermal readout and the released electrons can combine with holes trapped elsewhere. The energy released in the electron–hole recombination process is utilised for the excitation of Tb^{3+} ion, resulting in

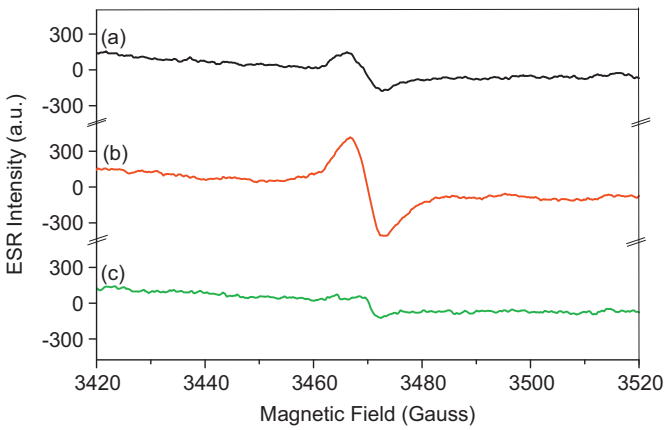

Fig. 11. Room temperature ESR spectra of irradiated $CaZrO_3:Tb^{3+}$ phosphor after thermal annealing at high temperatures. (a), (b) and (c) correspond to thermal anneal at 340 °C, 400 °C and 530 °C respectively. The spectra show the appearance, growth and decay of centre III (F^+ centre).

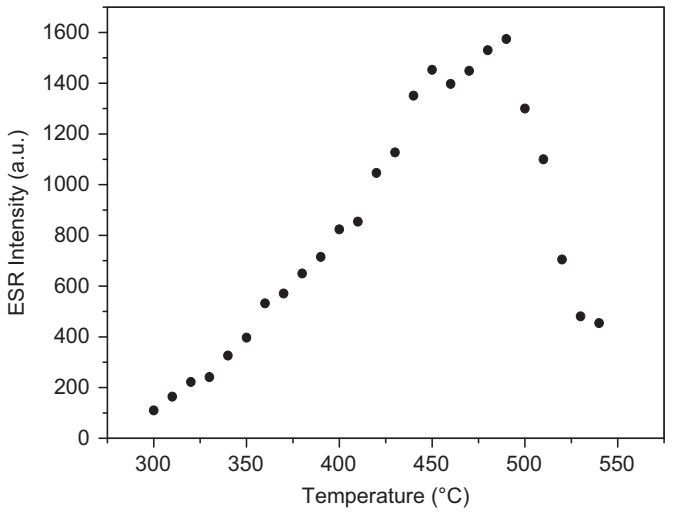

Fig. 12. Thermal annealing behaviour of centre III in $CaZrO_3:Tb^{3+}$ phosphor.

the TL peak. It is to be noted that the above mentioned appearance of F^+ centre at high temperature was also observed in our earlier study of Y_2O_3:Er phosphor [48].

4. Conclusions

Tb doped $CaZrO_3$ was synthesised via the combustion method using urea as the fuel element. It was characterised by XRD, FT-IR, and FE-SEM techniques. A green emission ($^5D_4 \rightarrow {}^7F_5$ at 545 nm) has been observed from the $CaZrO_3:Tb^{3+}$ powder phosphor under UV radiations. The $CaZrO_3:Tb^{3+}$ phosphor exhibits TL glow peaks at 126 °C, 200 °C and 480 °C. Three defect centres have been identified in the irradiated phosphor. These centres are tentatively assigned to an O^- ion and F^+ centres. O^- ion correlates with the 126 °C TL peak. One of the F^+ centres appears to act as a recombination centre for the peak at 126 °C and also correlates with the TL peak at 200 °C. The second F^+ centre seen after high temperature annealing and its precursor appear to be related to the TL peak at 480 °C.

Acknowledgements

Dr. Vijay Singh acknowledges the support of the Hanse-Wissenschaftskolleg, Delmenhorst, Germany. YDJ acknowledges the support from "Fusion-Tech. Developments for THz Info. & Comm." Programme of GIST. T.K. Gundu Rao is grateful to FAPESP, Brazil, for the research fellowship.

References

[1] N. Kurita, N. Fukatsu, K. Ito, T. Ohashi, J. Electrochem. Soc. 142 (1995) 1552.
[2] N. Sata, K. Hiramoto, M. Ishigame, S. Hosoya, N. Niimura, S. Shin, Phys. Rev. B 54 (1996) 15795.
[3] T. Higuchi, T. Tsukamoto, N. Sata, K. Hiramoto, M. Ishigame, S. Shin, Jpn. J. Appl. Phys. 40 (2001) 4162.
[4] R. Droopad, Z. Yu, J. Ramdani, L. Hilt, J. Curless, C. Overgaard, J.L. Edwards Jr., J. Finder, K. Eisenbeiser, W. Ooms, Mater. Sci. Eng. B 87 (2001) 292.
[5] T. Higuchi, T. Tsukamoto, S. Yamaguchi, N. Sata, K. Hiramoto, M. Ishigame, S. Shin, Jpn. J. Appl. Phys. 41 (2002) 6440.
[6] T. Schober, J. Friedrich, J.B. Condon, Solid State Ion. 77 (1995) 175.
[7] H. Yugami, S. Matsuo, M. Ishigame, Solid State Ion. 77 (1995) 195.
[8] T. Yajima, K. Koide, H. Takai, N. Fukatsu, H. Iwahara, Solid State Ion. 79 (1995) 333.
[9] J.B. Goodenough, Rep. Prog. Phys. 67 (2004) 1915.
[10] H. Iwahara, T. Esaka, H. Uchida, N. Maeda, Solid State Ion. 3-4 (1980) 359.
[11] T. Yajima, K. Koide, N. Fukatsu, T. Ohashi, H. Iwahara, Sensors Actuators B14 (1993) 697.
[12] H. Matsumoto, S. Hamajima, H. Iwahara, J. Electrochem. Soc. 135 (2001) D121.
[13] K.D. Kreuer, E. Schonherr, J. Maier, Solid State Ion. 70–71 (1994) 278.
[14] B. Gross, J. Engeldinger, D. Grambole, F. Hermann, R. Hempelmann, Phys. Chem. Chem. Phys. 2 (2000) 297.
[15] T. Schober, H.G. Bohn, Solid State Ion. 127 (2000) 351.
[16] M. Pollet, S. Marinel, G. Desgardin, J. Eur. Ceram. Soc. 24 (2004) 119.
[17] K. Kiyoshi, Y. Shu, I. Yoshiaki, Solid State Ion. 108 (1998) 355.
[18] T. Yamagushi, Y. Komatsu, T. Otobe, Y. Murakami, Ferroelectrics 27 (1980) 273.
[19] S.K. Manik, S.K. Pradhan, J. Appl. Crystallogr. 38 (2005) 291.
[20] Abdul-Majeed Azad, Mater. Lett. 60 (2006) 67.
[21] G. Rog, M. Dudek, A. Kozlowska-Rog, M. Bucko, Electrochim. Acta 47 (2002) 4523.
[22] W. Engelen, A. Buekenhoudt, J. Luyten, F. De Shutter, Solid State Ion. 96 (1997) 55.
[23] Y. Suzuki, P.E.D. Morgan, T. Ohji, Mater. Sci. Eng. A-Struct. 304–306 (2001) 780.
[24] J. Kung, R.J. Angel, N.L. Ross, Phys. Chem. Miner. 28 (2000) 35.
[25] E. Pinel, P. Boutinaud, R. Mahiou, J. Alloys Compd. 380 (2004) 225.
[26] Bing Yan, Xiaowen Cai, Xiuzhen Xiao, J. Fluoresc. 19 (2009) 221.
[27] Yuhei Shimizu, Sho Sakagami, Katsuhiko Goto, Yutaka Nakachi, Kazushige Ueda, Mater. Sci. Eng. B 161 (2009) 100.
[28] S.R. Jain, K.C. Adiga, V.R.Pai Vernekar, Combust. Flame 40 (1981) 71.
[29] Leen van Rij, Louis Winnubst, Le Jun Joop Schoonman, J. Mater. Chem. 10 (2000) 2515.
[30] T. Yu, C.H. Chen, Y.K. Lu, X.F. Chen, W. Zhu, R.G. Krishnan, J. Electroceram. 18 (2007) 149.
[31] W.S. Lee, C.Y. Su, Y.C. Lee, S.P. Lin, Tony Yang, Jpn. J. Appl. Phys. 45 (2006) 5853.
[32] S. Radovanovic, Proceedings of the 5th UNITECR'97, New Orleans, USA, 1997, p. 1613.
[33] C.S. Prasanth, H. Padma Kumar, R. Pazhani, Sam Solomon, J.K. Thomas, J. Alloy. Compd. 464 (2008) 306.
[34] C.H. Perry, D.J. McCarthy, G. Rupprecht, Phys. Rev. 138 (1965) 1537.
[35] T. Yu, W.G. Zhu, C.H. Chen, X.F. Chen, R.Gopal Krishnan, Physica B 348 (2004) 440.
[36] I.Erkin Gonenli, Cuneyt Tas, J. Eur. Ceram. Soc. 19 (1999) 2563.
[37] P.R. Krishnamoorthy, P. Ramaswamy, B.H. Narayana, J. Mater. Sci.—Mater. Electron. 3 (1992) 176.
[38] S. Serena, M.A. Sainz, A. Caballero, J. Eur. Ceram. Soc. 29 (2009) 2199.
[39] H. Zhang, X. Fu, S. Niu, Q. Xin, J. Lumin. 128 (2008) 1348.
[40] A. Zhang, M. Lü, G. Zhou, Y. Zhou, Z. Qiu, Q. Ma, J. Alloys Compd. 468 (2009) L17.
[41] H. Yamamoto, M. Mikami, Y. Shimomura, Y. Oguri, J. Lumin. 87–89 (2000) 1079.
[42] R.C. Weast (Ed.), CRC, Cleveland, 1971.
[43] H.J.A. Koopmans, G.M.H. Van De Velde, P.J. Gellings, Acta Crystallogr. C 39 (1983) 1323.
[44] G.P. Summers, G.S. White, K.H. Lee, J.H. Crawford, Phys. Rev. B21 (1980) 2578.
[45] J.M. Costantini, F. Beuneu, D. Gourier, C. Trautmann, G. Calas, M. Toulemonde, J. Phys.: Condens. Matter 16 (2004) 3957.
[46] A.I. Popov, E.A. Kotomin, J. Maier, Nucl. Instr. Methods B 268 (2010) 3084.
[47] M.G. Jani, R.B. Bossoli, L.E. Halliburton, Phys. Rev. B27 (1983) 2285.
[48] Vijay Singh, Vineet Kumar Rai, Isabelle Ledoux, S. Watanabe, T.K. Gundu Rao, J.F.D. Chubaci, Laurent Badie, Fabienne Pelle, Svetlana Ivanova, J. Phys. D 42 (2009) 065104.